Recording and Evaluation Methods of PIV Investigations on a Helicopter Rotor Model

by
M. Raffel[1], H. Richard[1], G. Schneider[1], F. Klinge[1], K. Ehrenfried[1], K. Pengel[2], G. Feenstra[2]

1) Institut für Aerodynamik und Strömungstechnik, DLR, Bunsenstraße 10, 37073 Göttingen, Germany
2) Large Low speed Facility LLF, DNW, Forsterweg 31, 8316 PR Marknesse, The Netherlands

Abstract Particle image velocimetry (PIV) experiments have been performed in order to derive quantitative flow velocity data of rotor blade tip vortices of a large-scale helicopter model and during a three weeks wind tunnel test. Today, three-component PIV wind tunnel tests at moderate speeds and observation distances can be performed on routine basis. The wind tunnel experiments, on which we will report, have been performed on a rotor model of 4m diameter in the 6m x 8m open test section of the Large Low-speed Facility (LLF) of the German-Dutch Wind Tunnel (DNW) operated at 33m/s. The rotor model used was a 40% Mach scaled model of the MBB Bo105 of the German aerospace establishment DLR in Braunschweig. The rotor consists of four hingeless blades with 0.121m chord length, rectangular blade planform, and -8° linear twist. The airfoil was a NACA 23012 with tabbed trailing edge. During the test, the model was mainly operated in descent flight conditions where blade vortex interaction dominates the noise emission. The rotor rotational frequency was 17.35Hz leading to a tip speed of 218m/s**.** The PIV system consisted of five digital cameras and three double pulse Nd:YAG lasers with 2x320mJ each, which were mounted onto a common traversing system in order to keep the distance between the cameras and the light sheet constant while scanning the rotor wake. The length of the traversing system was in the order of 10m, the height approximately 15m. More than half a Tera Byte (650GB) of PIV raw data had been recorded at various positions on the advancing and the retreating side. The measurements have been performed in the frame of the HART II program (Y. Yu 2002) and include noise, blade pressure, blade deformation and flow data by means of PIV. This paper focuses on the technical aspects of recording and evaluation of the 3-C PIV.

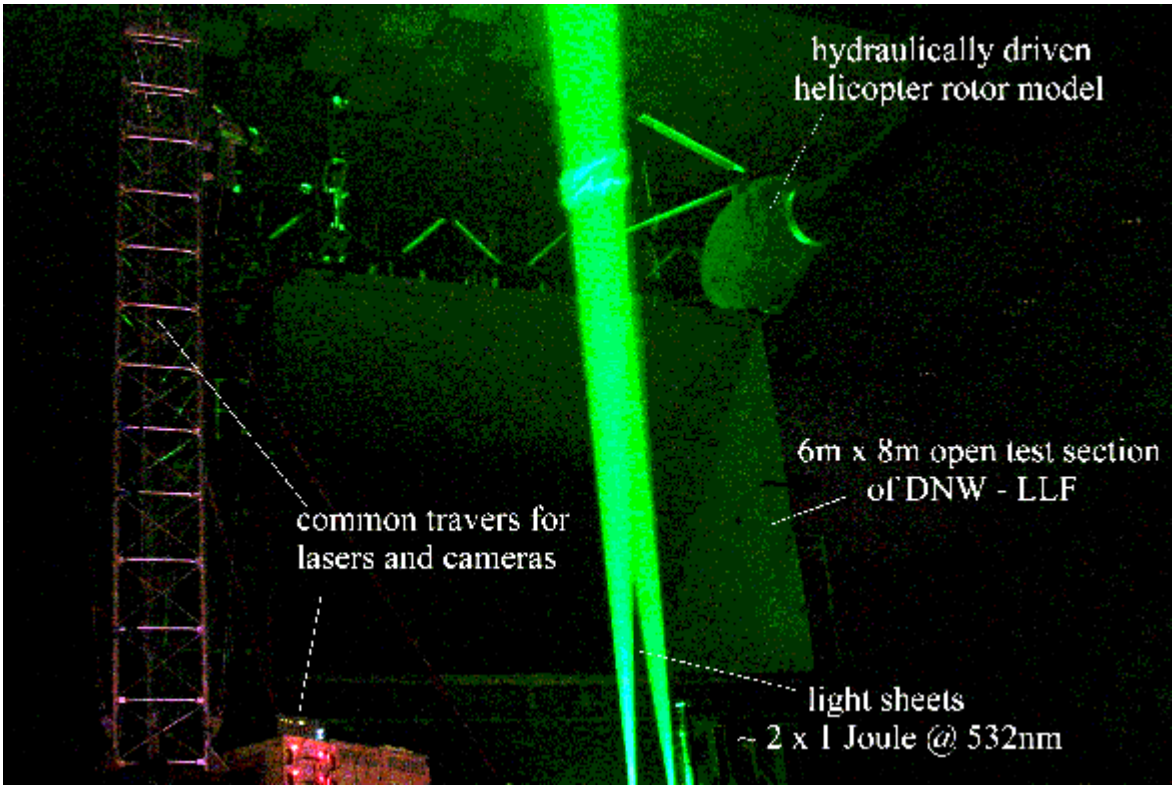

Figure 1: Experimental setup during PIV recording

In figure 1 the setup of the PIV measurements is shown. The upright structure of the common support, on which the cameras were mounted, can be seen on the left hand side. Three double pulse laser systems and the light sheet optics were mounted on the lower part of the support system. The PIV systems were synchronized to the rotor azimuth. With this equipement, the entire rotor disk was scanned for tip vortices on the advancing and retreating side.

INTRODUCTION

With increasing use of civil helicopters the problem of noise emission has become increasingly important within the last decades. Blade vortex interactions (BVI) have been identified as a major source of impulsive noise. As BVI-noise is governed by the induced velocities of tip vortices, it depends on vortex strength and miss-distance, which itself depends on vortex location, orientation, and convection speed relative to the path of the advancing blade. Blade vortex interaction can occur at different locations inside the rotor plane depending on flight velocity and orientation of the blade tip path plane. Numerical simulations of the acoustic near and far-field (e.g. Ehrenfried et al. 1991, Burley et al. 1991) are based on the interaction of the blades with vortices, which were described by mathematical models. Due to the complexity of the flow field under investigation, more sophisticated aerodynamic simulations like e.g. RANS computations can not be included. Therefore, aero-acoustic rotor simulations depend on experimentally obtained flow field data in order to derive appropriate vortex models and to validate the simulation of the vortex flight path and aging. Since the vortex structure considerably depends on Reynolds number (see e.g. Splettstößer et al. 1984, Caradonna et al. 1988, McCroskey 1995, Leishman and Bagai 1996) remarkable efforts are taken in order to obtain flow field data at large scales (e.g. Splettstößer et al. 1995, Raffel et al. 1998). It is understood, that the study of these phenomena is of particular interest for progress towards quieter helicopters. The measurement technique described here, has been applied during the international HART II project undertaken by NASA, US-Army, ONERA, DNW, and DLR (Y. Yu et al, 2002).

RECORDING

Flow seeding

The flow seeding has been performed by Laskin nozzle particle generators. The DEHS particles had a mean diameter below 1μm. A distributor rake has been used. It was mounted in the settling chamber of the wind tunnel on a traverse in order to guide a homogeneously seeded stream tube into the observation area. In figure 2 the seeding rake and a typical example of a PIV image is presented which shows that it is possible to seed the blade tip vortex. However, the seeding density inside the vortex core is lower than in the overall flow field.

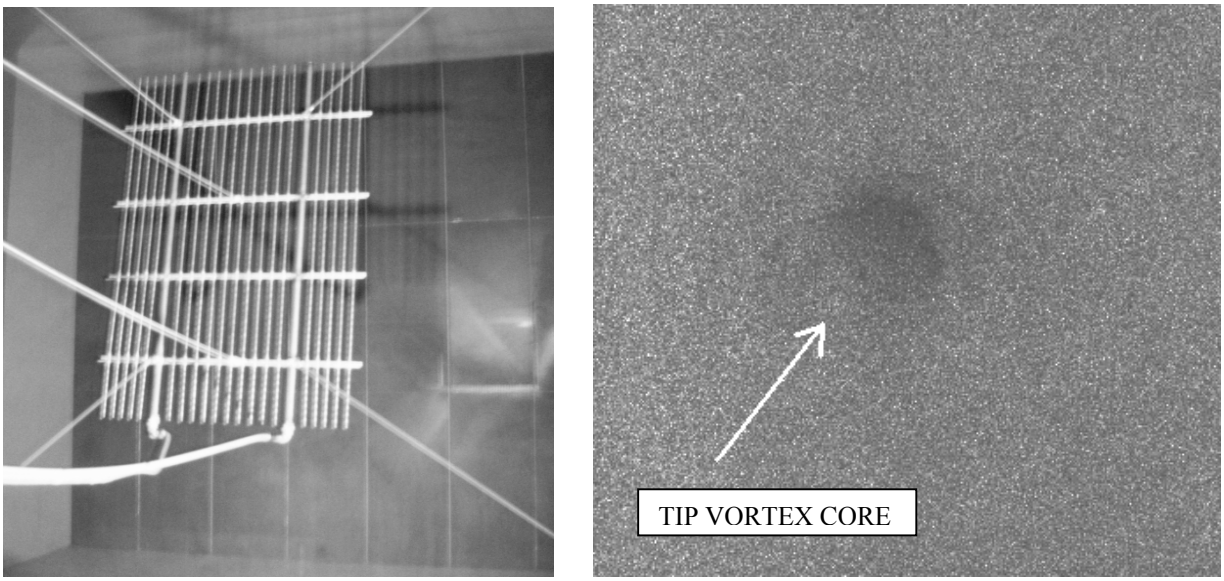

Figure 2: The distribution of seeding particle in the settling chamber and in the test section

Two stereoscopic PIV systems have been used in order to obtain one large and one smaller observation area. A fifth camera has been used in order to check the seeding distribution in the light sheet and to detect the vortex. Each camera has a resolution of 1024 by 1280 pixels and a sensor cooling which reduces the black current and increases the dynamics range which is digitized to 12 bit. The cameras were mounted onto a traverse system described below and were connected to computers by fiber optics. Each of them was equipped with a remotely controlled focusing device. One of the stereoscopic systems was equipped with 100mm lenses in order to have a large observation area and the second system with 300mm lenses to investigate the tip vortex with a high spatial resolution. The cameras were installed on a tower and each pair was separated vertically by 5.2m. The horizontal distance between the cameras and

the light sheet was 5.6m. One camera from both sets with the vertical traverse can be seen on figure 4: The lower one with a 100mm lens and the upper one with a 300mm lens. The cameras as well as the lasers were synchronized with a one-per-rev signal given by the rotor, which allows to phase lock the recording at a desired phase-angle of the rotor blade. The principle of this synchronization is illustrated in figure 3.

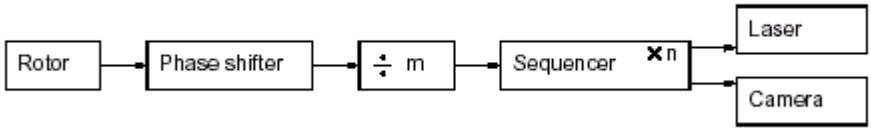

Figure 3: Diagram of trigger system for rotor-laser synchronization.

Table 1: Example solution for rotor-laser synchronization.

rotor	laser flash lamps.	rotor/flash lamp	camera and q-switch.
1041 RPM ~ 17.35Hz	9.914Hz	7/4	2.479Hz

A "one per revolution" trigger signal from the rotor was taken and passed to a so-called phase shifter. This phase shifter delays the incoming signal. The delay time is computed from the actual rotor period and a given phase shift. Due to the constant rotor frequency, a very accurate and stable phase shift could be achieved.

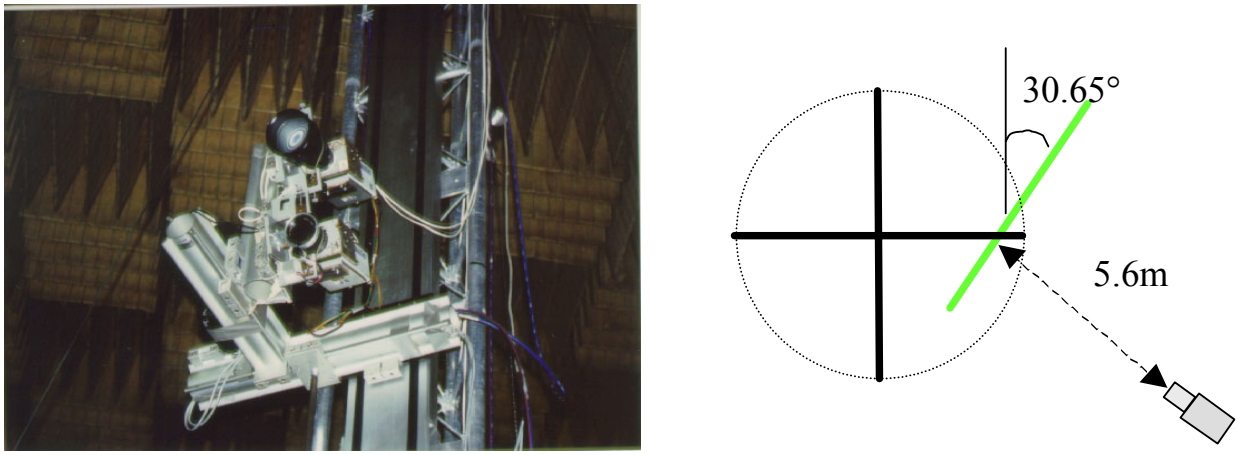

Figure 4: PIV cameras and viewing direction (flow from above)

Cameras and light sheet traverses

Cameras, lasers and light sheet optics have been mounted onto a traversing system, the so-called common support system of DNW-LLF. In this set-up the distance between cameras and light sheet could be kept constant during all PIV measurements. A pixel-to-length re-calibration and a camera alignment, which has usually to be applied after set-up changes, could be avoided. Additional traverses were mounted to the tower on the common support in order to move the cameras up and down (z-direction) parallel to the light sheet.
The common support is a three-axis traversing system, two lateral axes (in x- and y-direction) and one (vertical) rotation axis (see figure 5). Together with the camera traverses every required measuring position on the "advancing side" of the rotor could be reached without replacing the common support.

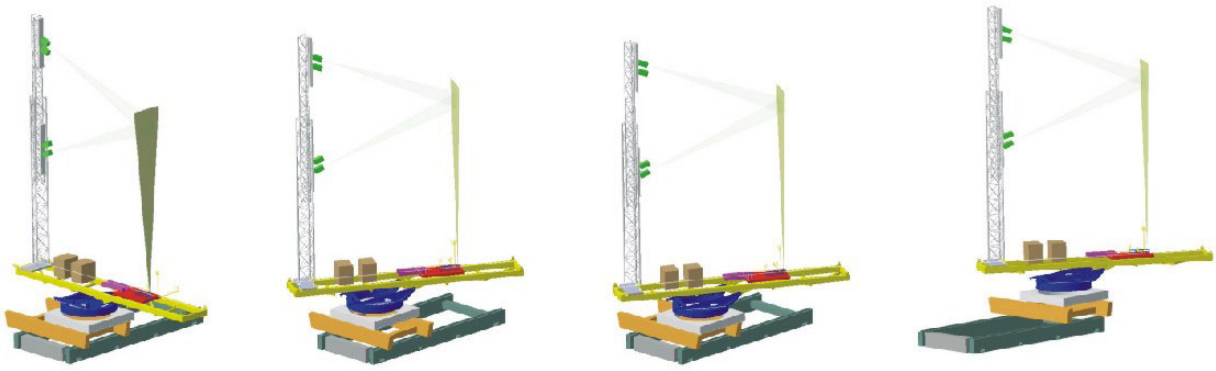

A B C D

Figure 5 Common Support (appr. 14 m x 10 m x 3 m) with PIV set-up in origin position (A), rotated (B), traversed in x-direction (C) and traversed in y direction (D).

However, before the measurements on the retreating side of the rotor, the tunnel had to be stopped and the common support was moved to the portside of the model. The axes of the different traverses were calibrated, in a way that the displayed and recorded position is the position of the PIV reference point in the tunnel co-ordinate system. The PIV reference point was a defined position in the center of the PIV images, which has been measured by means of theodolites prior to PIV calibration.

Helicopter model and test condition

The wind tunnel experiments have been performed during the HART II campaign on a Bo105 model rotor. The rotor consists of four blades with 0.121m chord length and has a diameter of 4m with a tip speed of 218m/s (1040 rpm). All the PIV equipment (laser, cameras) was mounted on a remotely controlled traverse (figure 5) which allows to scan the complete rotor disk without changing the setup. The light sheet was generated by 3 double pulsed Nd: YAG laser system which allowed to have a large (≈1.5m) and also thick light sheet (≈7mm). It was oriented with an angle of 30.6° with respect to the wind tunnel axis (see figure 4).

EVALUATION

Before cross-correlation of the dewarped recordings, the particle images passed several filters:

- High pass filter: the high pass filter of the image was performed by subtracting a low pass filtered version of the input image. The kernel size of the low pass filter was set to be 7x7 pixel.
- Binarization: the pixel values above the specified threshold of 7 were set to white and lower values to black.
- Anti-alias: a 2x2 pixel low pass filter was applied which damps out spurious noise in the image.

The combination of the three filters significantly helped when images with low contrast had to be evaluated (recorded during the failure of one of the laser system). These recordings were processed using the correlation technique presented by D..P. Hart, (Hart 1998) with an interrogation window size of 32x32 pixel for the large field of view and 32x32 pixel and additionally 24x24 pixel for the small field of view with 50% overlap in each case.
The recordings that have been performed with the full laser power (3x320mJ per pulse) have been processed in the same way. Here, the use of image filtering and of the 'Hart-correlation' allowed us to use smaller interrogation windows down to 16x16 pixel which yields to an improvement of 50% in terms of spatial resolution in length, compared to the 24x24 pixel interrogation windows. The effect of the windows size can be seen later on figures 11 to 13 which represent horizontal and vertical cut through the vortex center using three different interrogation window sizes: 24, 20 and 16 pixel. This increase of spatial resolution yields to slightly higher peak-to-peak velocities and to a 50% higher peak vorticity.

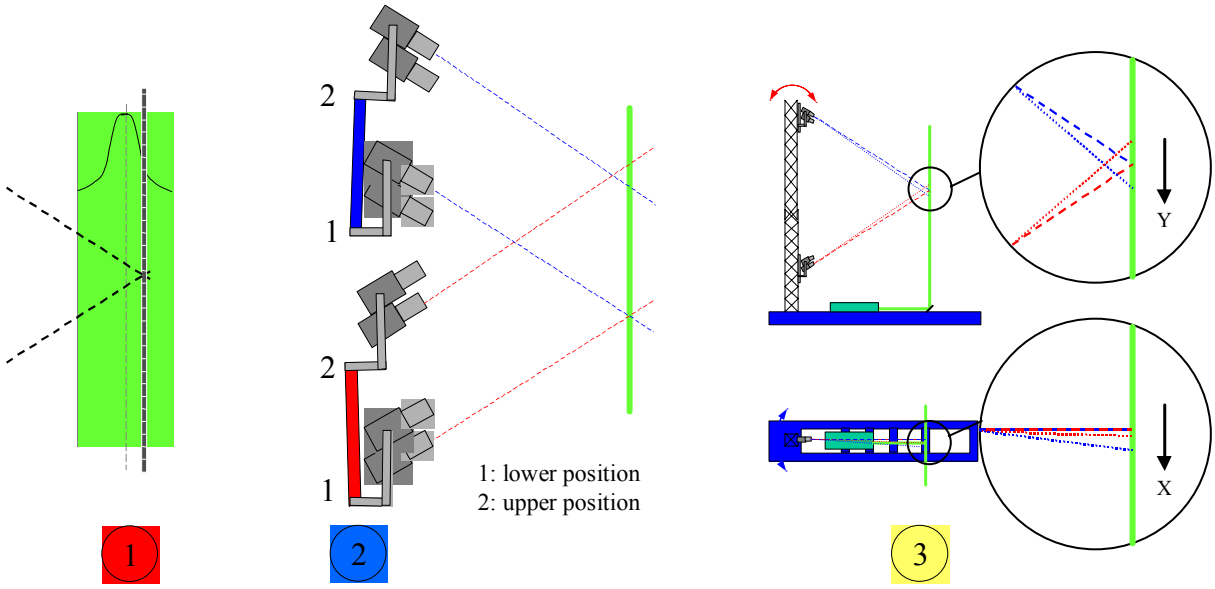

Figure 6: Sources of errors

The stereoscopic PIV recording in large industrial facilities requires a sophisticated calibration scheme and a refinement of the dewarping of the recordings. In the case of strong velocity gradients, like in the blade tip vortices measured here, a very small misalignment in the order of a millimeter would lead to severe errors during the reconstruction of the out-of-plane velocity component. Traverse dimensions of more than 10m on the other hand do not allow to completely avoid such a small miss-alignment. Three different mechanisms have been identified to be the main sources of errors (figure 6):

(1) The exact location of the calibration grid in the light sheet does not necessarily correspond to the location of the mean intensity of the light sheet, which has usually no regular intensity profile.
(2) The mounting of the camera traverses in 10m height introduces a small miss-alignment and was not perfectly parallel with respect to the light sheet.
(3) Very small vibrations due to turbulences in the open test section of the large wind tunnel facility introduce a small displacement of the viewing field of the upper and the lower cameras.

Therefore, a cross-correlation between the dewarped single exposed images from each camera pair in stereoscopic imaging configuration acquired at the same instance of time has been computed in order to obtain the local misalignment between the images. Any serious misalignment due to translation, rotation or deformation (magnification change of one image) can be found and corrected by a re-computation of the dewarping coefficients. This easy elimination of residual alignment errors can be done, because the dewarping is performed before the cross-correlation for velocity determination.

In the following, we summarize the general outline of the evaluation scheme.

The steps of the evaluation are respectively:

- The determination of the dewarping coefficients using the calibration grid.
- The image pre-processing and the dewarping of the PIV recordings.
- The correction of the dewarping coefficients using the result from the cross-correlation from a single exposed recording from different cameras.
- The final dewarping of the PIV raw data.
- The cross-correlation of the two exposures of each camera.
- The outliers detection.
- The computation of the 3-C results according to the location of the cameras.
- The post-processing: units conversion, re-origin, computation of differential operators.

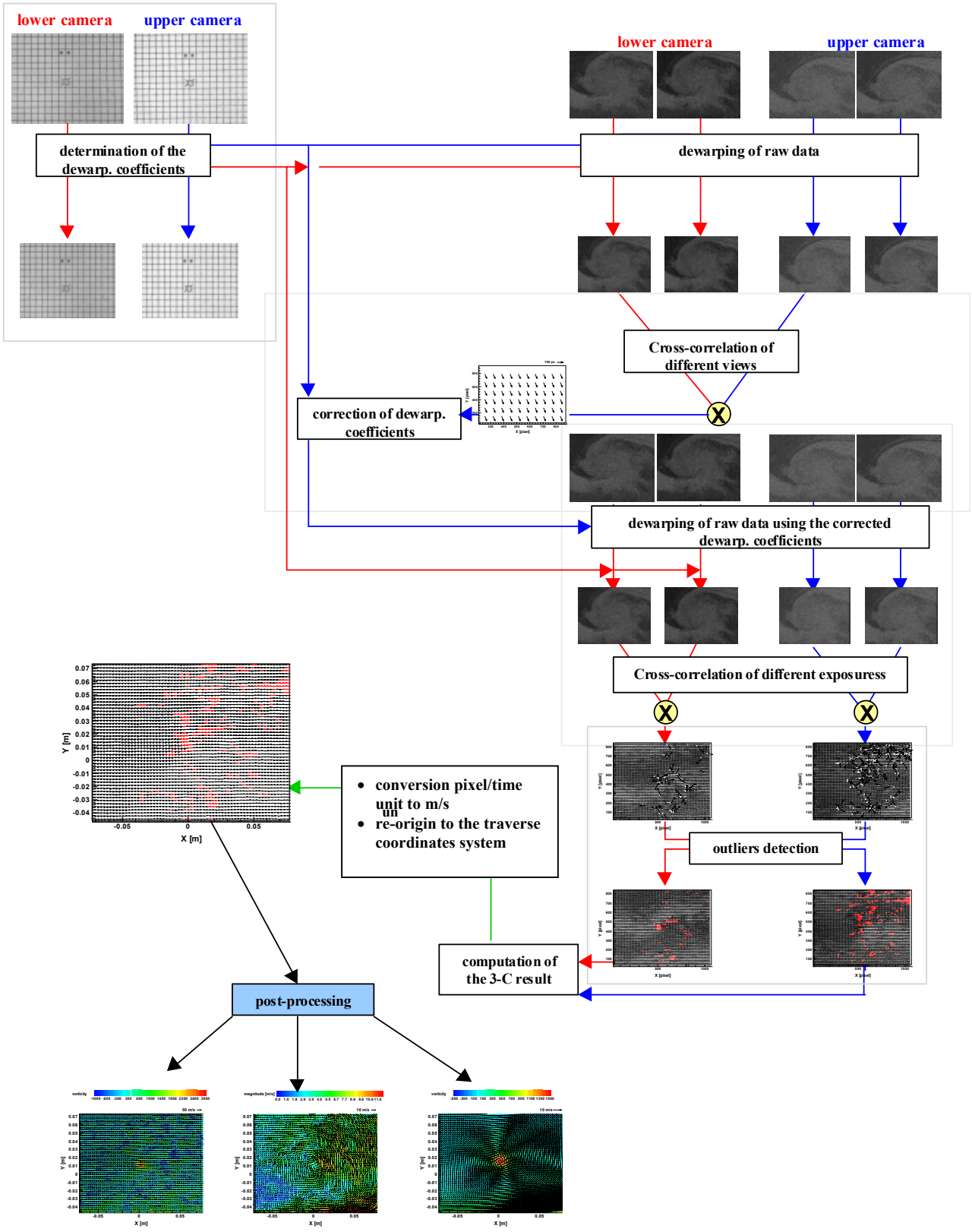

Figure 7: Flow chart of the PIV processing

ACCURACY ESTIMATIONS

The overall measurement accuracy in PIV in general is a combination of a variety of aspects.

The absolute measurement error in the estimation of a single displacement error, ε_x, can be decomposed into the bias error, ε_{bias}, and a random error or measurement uncertainty ε_{rms}.

The contributing factors of the measurement uncertainty and systematic errors will shortly be described in the following. Their influence has been tested most frequently by Monte Carlo simulation by various authors (e.g. Keane and Adrian 1992). The estimates of the measurement uncertainties used in the following were taken from diagrams presented by C. Willert in reference Raffel et al. (1998).

When using Gaussian peak approximators the optimum **particle image diameter** is slightly more than two pixels for the cross-correlation evaluation. We found constant average image diameters of 2 – 3 pixel for all test parameters. For larger values the random noise ε_{rms} is increasing. When the particle images become too small an effect arises, which has most frequently been described as peak locking. In this case, the displacement tends to be biased towards integer pixel values, resulting in an increased bias error, ε_{bias}. The peak locking effect is, from the author's experience, one of the main drawbacks of digital PIV. Beside particle image size it depends on many other parameters e.g. the peak estimator used. It can frequently be observed by plotting a displacement histogram. However, in the data sets recorded and evaluated in the frame of the HART II project no peak locking has been detected.

The **interrogation window size** is the second important influence on the uncertainty of the displacement estimate. According to Raffel et al. (1998), the random noise increases from 0.01 pixel at a 64 pixel window size to 0.1 pixel at a 16 pixel window size. In order to reach a small sampling area and a high spatial resolution, but also data with a reduced noise component we decided to evaluate with up to four different window sizes.

The reason for using different interrogation window sizes is, that the amount of measurement noise and spatial resolution, which can be accepted depends on the physical quantity investigated and on the post-processing procedure used. The out-of-plane component e.g. contains more noise than the in-plane component because it is computed from the difference of the measured in-plane components. When computing ensemble averages of the samples, the stronger spatial averaging of a large interrogation window size might not be needed. Additionally, the development and improvement of post-processing routines is probably continuing over the next years and is different for different users. The effect of the different sampling sizes (interrogation window) will be shown later.

Monte Carlo simulations indicated that the **image quantization** has only little influence on the measurement uncertainty or displacement bias error. Therefore, the dynamic range of the 12 bit converter of the cameras has not been fully used, but the light sheet thickness has been extended in order to allow larger pulse separation times. The resulting intensities of the particle images were therefore only 2 – 3 times higher than the background noise and have been binarized prior to correlation (see above). This leads to RMS-uncertainties, which are comparable to cases of no noise and high image exposure. The **background noise level** itself was very low due to sensor cooling, dark ambient conditions and the absence of model reflections in the image background.

Due to the small interrogations window used and the relatively small observation window, the **displacement gradients** were small over most areas of the recordings. However, due to the strong velocity gradients and a reduced particle density inside the vortex core, the RMS-uncertainty of displacements measured inside the core might reach values of 0.1 pixel in the worst cases of the measurement campaign.

Beside that is has to be stated, that even with relative high magnifications during the recording and the small window sizes during evaluation the peak values inside the vortex core are damped due to the spatially averaging nature of the statistical PIV evaluation (Martin and Leishman 2001). More efforts are needed in order to quantitatively determine this effect and/or reduce this effect by the development of better algorithms.

The measurement of the blade tip vortices lead to a significantly strong out-of-plane flow component. As described by Keane & Adrian (1992), the **out-of-plane loss of pairs** can reduce the correlation peak signal strength such that the measurement noise increases significant and the detection probability increases strongly. Therefore, the out-of-plane loss of pairs should be limited by reducing the out-of-plane particle displacement to 1/3 of the light sheet thickness ΔZ.

A careful analysis of the HART II data lead to the following estimates of the displacement error: the random noise error is smaller than 0.05 pixel for all the observation area except the vortex core of vortices with strong velocity gradients were it could reach 0.1 pixel.

The bias errors, which we were not able to compensate for, is the error due to the peak locking effect described above. Since displacement histograms gave no indication of accumulations of measured integer pixel displacements we can state, that the bias error is at least significantly smaller than the random noise error and therefore smaller than 0.05 pixel in most cases.

Due to the recording conditions displayed an estimated error in the displacement estimation corresponds to a certain measurement error in the velocity domain. The measurement error ε_u is given by $\varepsilon_u = \varepsilon_x / (\Delta t \cdot M)$ wherein Δt is the pulse separation time and M the magnification during recording. The measurement error relative to full scale[1] is $\varepsilon_{u,\,rel} = \varepsilon_u / U_{max}$. When limiting the maximum out-of-plane particle displacement by an appropriate setting of the pulse separation time, the following formula can be found for every PIV measurement:

$$\varepsilon_{u,\,rel} \leq W_{max} / U_{max} \cdot 3/(\Delta Z \cdot M) \cdot \varepsilon_{x,}$$

wherein,

W_{max}	is the maximum out-of-plane component of the flow velocity,
U_{max}	is the maximum in-plane component of the flow velocity,
ΔZ	is the light sheet thickness,
M	is the magnification, and
ε_x	is the displacement measurement error in physical dimensions.

Therefore, the measurement error has to be minimized by the minimization of the three factors: W_{max} / U_{max}, $3/(\Delta Z \cdot M)$, and ε_x. In the recording situation described above the ratio W_{max} / U_{max} was, on one hand dominated by the wind tunnel mean flow and its decomposition into the in-plane and out-of-plane components, and the tangential velocities of the blade tip vortices on the other hand. During most of the test, the ratio was $W_{max} / U_{max} \sim 1$. It could not be further minimized by a different orientation of the light sheet plane, because this was given by the wind tunnel geometry and the aim to cut the vortices as much orthogonal as possible to their axis.

By the combination of three double pulsed laser systems with 320 mJ per pulse each, due to the sensitive cameras with cooled CCD arrays and the forward / backward scatter arrangement we were able to reach a light sheet thickness between 5 mm (during the failure of one of the laser systems) and 8 mm with a width of approximately 1.5m. The magnification varied from appr. 1/20 for the 300 mm lenses down to appr. 1/60 for the 100 mm lenses.

The relative measurement error of the best cases and worst case respectively has been estimated by taking the following parameters into account:

best
$W_{max} = 100$m/s,
$U_{max} = 100$m/s,
$\Delta Z = 8$mm,
M = 1/20,
$\varepsilon_x = 0.1\text{px} \cdot 6.7 \cdot 10^{-6}$m/px.

worst
$W_{max} = 100$m/s,
$U_{max} = 100$m/s,
$\Delta Z = 5$mm,
M = 1/60,
$\varepsilon_x = 0.2\text{px} \cdot 6.7 \cdot 10^{-6}$m/px.

This leads to a relative error of the measured in-plane velocity of:

$\varepsilon_{u,\,rel} \leq 0.5\text{ms}^{-1} / U_{max} = 0.5\%$ (best case) and $\varepsilon_{u,\,rel} = 4.8\text{ms}^{-1} / U_{max} = 4.8\%$ (worst case)

[1] „full scale“ has been estimated by the maximum velocity measured of $U_{max} \sim 100$ m/s.

RESULTS AND DISCUSSION

Figures 8 and 9 show averaged vector and vorticity fields from the two stereoscopic pairs during baseline conditions (no higher harmonic control of the blades) at the advancing side of the rotor. The recordings were taken with $\Delta t=22\mu s$ between the exposures and were processed according to the procedure described above with interrogation windows sizes of 32x32 pixel for the large field of view and 24x24 pixel for the small field of view.
It can be seen, that the large field of view allows to capture the blade tip vortex but also the surrounding flow: the shear layer from a previous blade is clearly visible on the lower right corner. The larger magnification of the small field of view allows to capture the vortex with a relative high spatial resolution. This high spatial resolution is needed in order to get accurate vortex characteristics, the maximum of vorticity is, for example, 20% higher than that obtained with the large field of view.

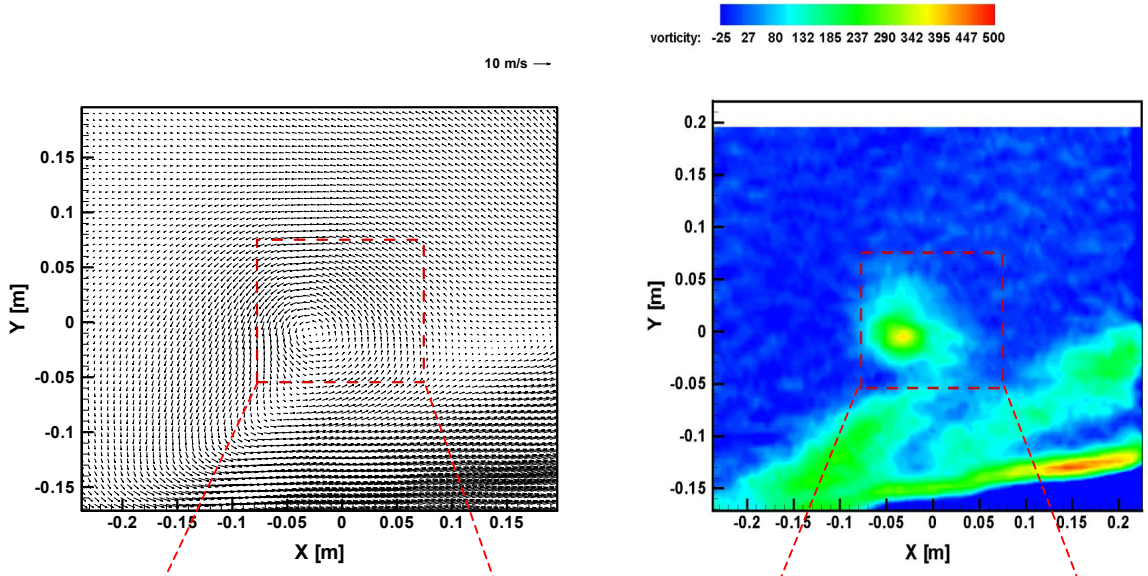

Figure 8: Simple averaged vector and vorticity fields from the large field of view (100mm lens)

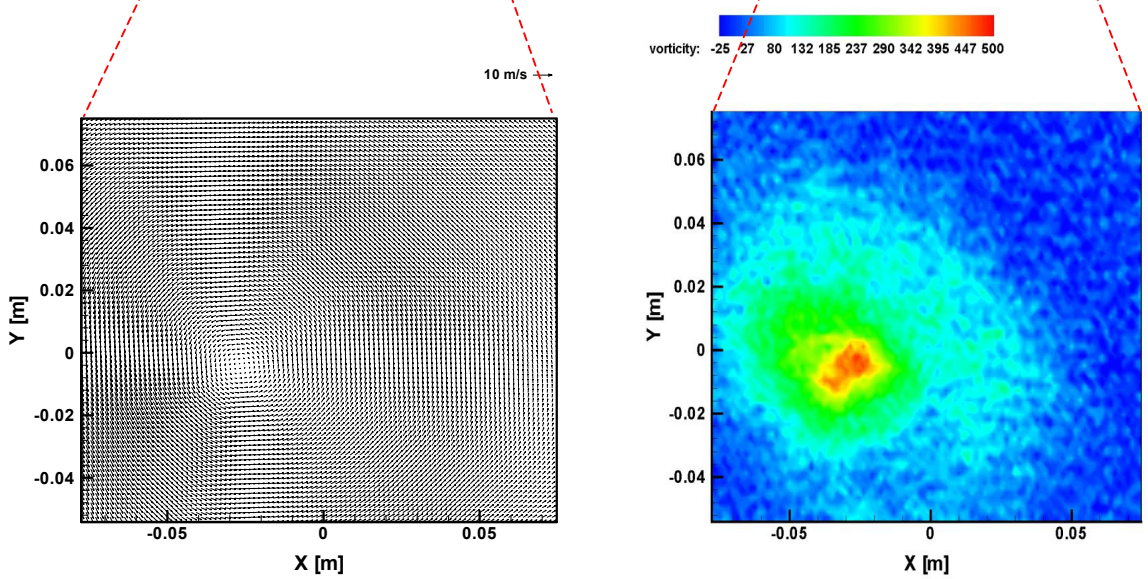

Figure 9: Simple averaged vector and vorticity fields from the small field of view (300mm lens)

The simple average (data in tunnel coordinates) presented on figures 8 and 9 enables to obtain the mean vortex location, but due to the vortex wandering, the vortex characteristics (peak-to-peak velocity, core size) are smoothed and spatially spread non-physically. In order to avoid this smoothing each result should be moved according to the vortex center before averaging (see e.g. Vogt et al. 1997 McAlister 2001). The averaged vector and vorticity fields obtained using such a method

are presented in figure 10. For each PIV vector field the vortex center has been found and relocated to the origin by using wavelet analysis algorithm developed by C. Schram (2001) at the von Karman Institute (Belgium). It can be seen on the averaged vector field, that the vortex is represented much more defined if the data is transfered into in vortex coordinates before averaging. The core size (peak-to-peak) is equal to 2cm whereas with a normal average it is equal to 10cm, and the vorticity maximum is more than three times higher. In spite of the difficult experimental conditions PIV data were obtained with relatively high spatial resolution.

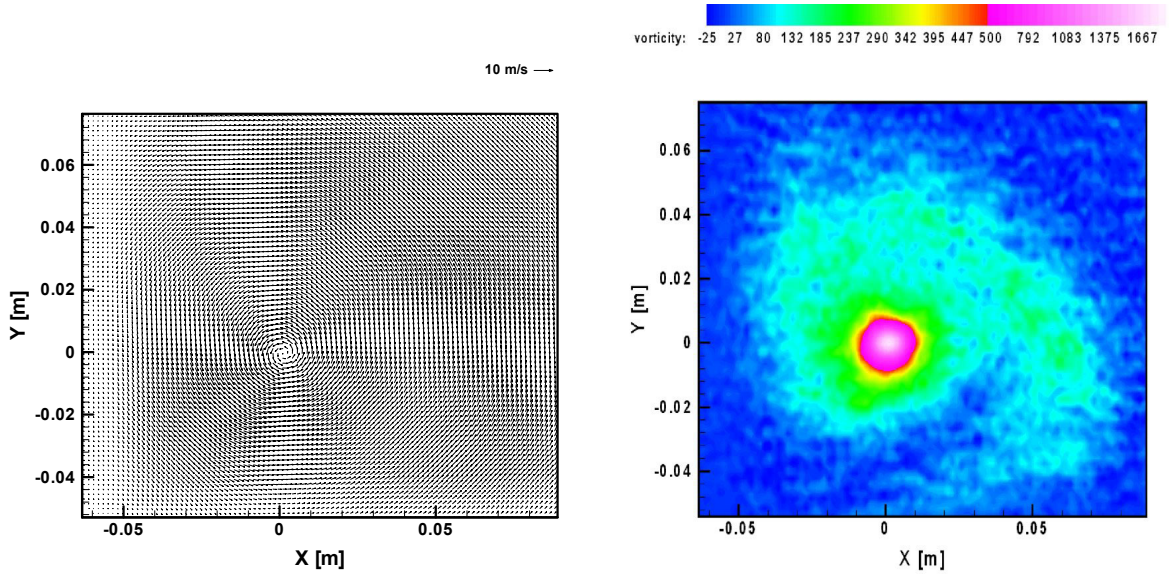

Figure 10: Corrected averaged vector and vorticity fields (data shifted with respect to the vortex center) from the small field of view

Complex flow field measurements with varying seeding densities and significant velocity gradients, does usually not allow to obtain very small interrogation window sizes. The interrogation window size we were aiming in the planning phase was 32 x 32 pixel Due to reasons stated above, we reduced the window size down to 16 pixel resulting in four times more statistically independent velocity vectors.

Advantages and disadvantages of small interrogation window sizes can be seen in figures 11 - 13: the peak values of the amplitude and gradient of the measured velocity and vorticity in the vortex core were obviously larger. On the other hand, the random noise component outside the vortex center increased.

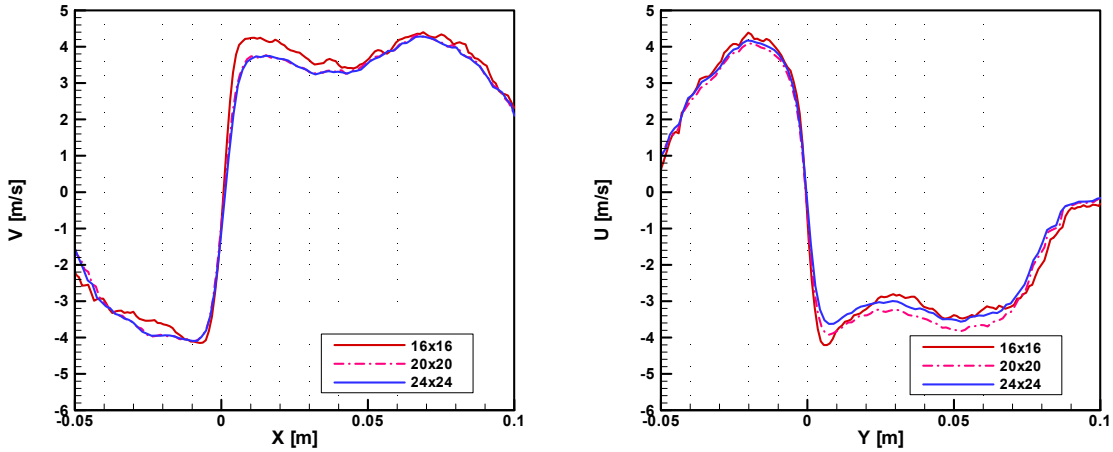

Figure 11: Horizontal and vertical velocity profile through the vortex center of figure 10

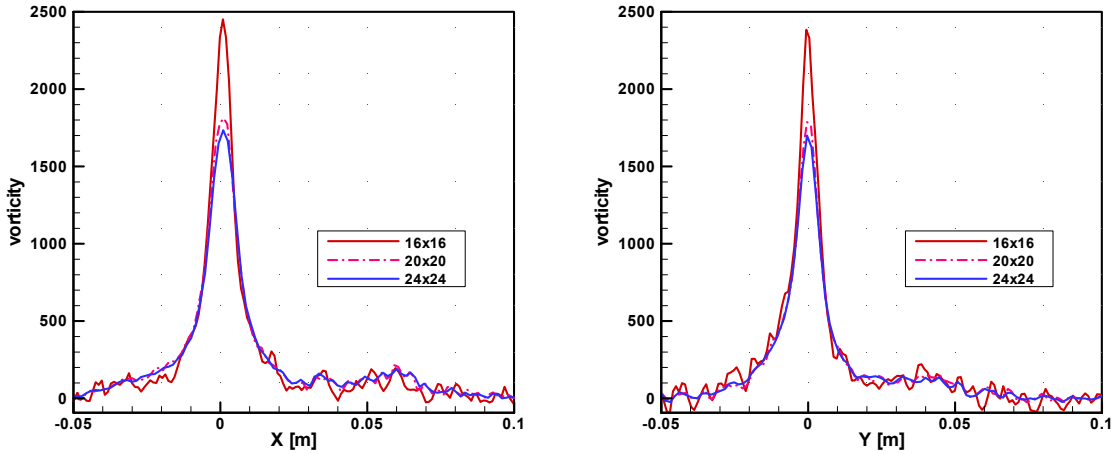

Figure 12: Horizontal and vertical vorticity profile through the vortex center of figure 10

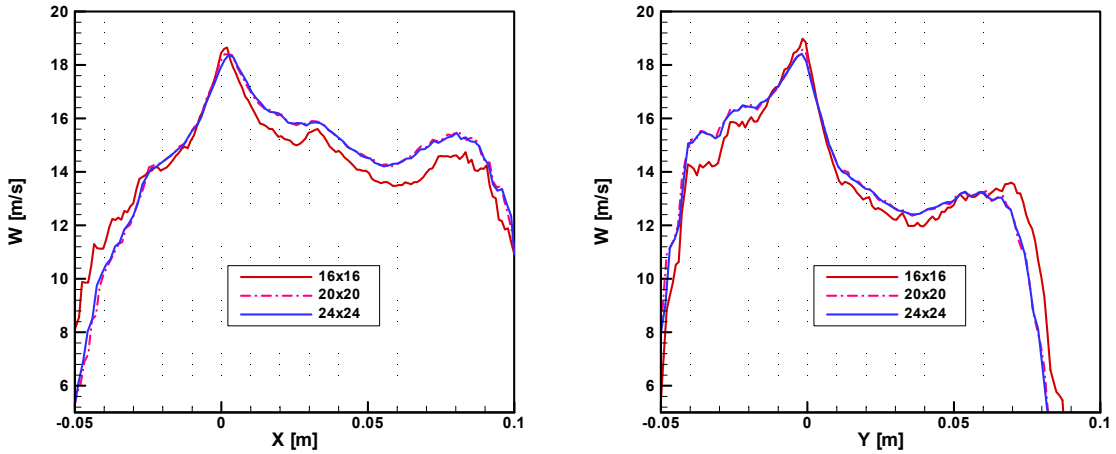

Figure 13: Horizontal and vertical out-of-plane velocity profile through the vortex center of figure 10

It can be concluded, that the PIV measurements yielded to interesting results concerning the structure of the blade tip vortices. In addition to geometric parameters like location of the vortex relative to the rotor plane, the vortex flight path through the rotor disk, the vortex core size, and velocity gradients have been derived to form a basis of a vortex development and aging model.

Acknowledgement

The authors would like to specially thank the engineers and technicians of DLR Braunschweig for their cooperation and all the people who took part in the measurements and C. Schram for his help and support in the vortex characteristics analysis. We highly appreciate the productive and excellent partnership of the HART II community, who gave us the opportunity to perform these measurements.

Literature

Burley C.L., Jones H.E., Marcolini M.A., Splettstößer W.R. 1991: "Directivity and prediction of low frequency rotor noise", *AIAA 91-0592*, Aerospace Science Meeting, Reno, USA.

Caradonna F.X., Lautenschläger J.L., Silva M.J. 1988: "An experimental study of rotor-vortex interaction", *AIAA 88-0045*, Aerospace Science Meeting, Reno, USA.

Ehrenfried K., Meier G.E.A., Obermeier F. 1991: "Sound produced by vortex-airfoil interaction", 17th European Rotorcraft Forum, Paper 63, Berlin, Germany.

Hart D.P: ."PIV Error Correction", 9th International Symposium on Applications of Laser Techniques to Fluid Mechanics, July 13-16, 1998, Lisbon, Portugal.

Leishman J.G., Bagai A. 1996: "Challenges in Understanding the Vortex Dynamics of Helicopter Rotor Wakes", AIAA Journal Vol. 36, No. 7, pp.1130-1140.

Martin P. B., Pugliese G. J, Leishman J.G. : "High resolution trailing vortex measurements in the wake of a hovering rotor", AHS 57th Annual Forum, Washington, DC, USA, May 2001.

McAlister K. W., Tung, C., Heineck J.T.: "Forced diffusion of trailing vorticity from a hovering rotor" AHS 57th Annual Forum, Washington, DC, USA, May 2001.

McCroskey W.J. 1995: "Vortex Wakes of Rotorcraft", paper 95-0530, 33rd AIAA Aerospace Sciences Meeting and Exhibit, Reno, USA.

Raffel, M.; De Gregorio, F.; Pengel, K.; Willert, C.; Kähler, C.; Ehrenfried, K.; Kompenhans, J., 1998: "Instantaneous flow field measurements for propeller aircraft and rotorcarft research", 9th Intl. Symposium on Appl. of Laser Techniques to Fluid Mechanics, Lisbon, paper 19.6.

Raffel, M.; Willert, C.; Kompenhans, J., 1998: "Particle Image Velocimetry, A Practical Guide", Springer-Verlag.

Schram C., Riethmuller M.L., 2001 "Vortex ring evolution in an impulsively started jet using digital image particle velocimetry and continuous wavelet analysis", Measurement Science and Technology (12), 1413-1421.

Splettstößer W.R., Schultz K.J., Bowwell D.A., Schmitz F.H. 1984: "Helicopter Model Rotor blade/vortex interaction impulsive noise; scalability and parametric variations", NASA TM 86007.

Splettstößer W.R., Kube R., Wagner W., Seelhorst U., Boutier A., Micheli F., Mercker E. 1995: "Key results from a higher harmonic control aeroacoustic rotor test (HART) in the German-Dutch wind tunnel", 21th European Rotorcraft Forum, St. Petersburg, Russia.

Vogt, A.; Baumann, P.; Gharib, M.; Kompenhans, J.; 1996, "Investigations of a wing tip vortex in air by means of DPIV", Proc. 19th AIAA Advanced Measurement and Ground Testing Technology, New Orleans, USA, paper AIAA 96-2254.

Yu Y.:. "The HART program, Joint International Rotor Aeroacoustics Test and Analysis Validation Program", AHS International Technical Specialist Meeting, San Francisco, USA, January 2002.

Yu Y., Tung C., van der Wall B., Pausder J, Burley C., Brooks T., Beaumier P., Delrieux Y., Mercker E.: " The HART-II Test: Rotor Wakes and Aeroacoustics with Higher-Harmonic Pitch Control (HHC) Inputs- The Joint German/French/Dutch/US Project -", AHS 58th Annual Forum, Montreal, Canada, June 2002.